J. Fluid Mech. (2006), *vol.* 556, *pp.* 361–386. © 2006 Cambridge University Press
doi:10.1017/S0022112006009712 Printed in the United Kingdom

Wave evolution on electrified falling films

By DMITRI TSELUIKO
AND DEMETRIOS T. PAPAGEORGIOU

Department of Mathematical Sciences and Center for Applied Mathematics and Statistics, New Jersey Institute of Technology, Newark, NJ 07102, USA

(Received 27 April 2005 and in revised form 10 November 2005)

The nonlinear stability of falling film flow down an inclined flat plane is investigated when an electric field acts normal to the plane. A systematic asymptotic expansion is used to derive a fully nonlinear long-wave model equation for the scaled interface, where higher-order terms must be retained to make the long-wave approximation valid for long times. The effect of the electric field is to introduce a non-local term which comes from the potential region above the liquid film. This term is always linearly destabilizing and produces growth rates proportional to the cubic power of the wavenumber – surface tension is included and provides a short wavelength cutoff. Even in the absence of an electric field, the fully nonlinear equation can produce singular solutions after a finite time. This difficulty is avoided at smaller amplitudes where the weakly nonlinear evolution is governed by an extension of the Kuramoto–Sivashinsky equation. This equation has solutions which exist for all time and allows for a complete study of the nonlinear behaviour of competing physical mechanisms: long-wave instability above a critical Reynolds number, short-wave damping due to surface tension and intermediate growth due to the electric field. Through a combination of analysis and extensive numerical experiments, we find parameter ranges that support non-uniform travelling waves, time-periodic travelling waves and complex nonlinear dynamics including chaotic interfacial oscillations. It is established that a sufficiently high electric field will drive the system to chaotic oscillations, even when the Reynolds number is smaller than the critical value below which the non-electrified problem is linearly stable. A particular case of this is Stokes flow.

1. Introduction

Falling films have received much attention since the pioneering experiments of Kapitza & Kapitza (1949) (also Binny 1957). Applications can be found in a wide variety of technological processes including coating and cooling. In cooling applications, for example, it has been observed that heat or mass transfer can be increased by an order of magnitude if there are waves present on the liquid film (Dukler 1976; Yoshimura, Nosoko & Nagata 1996; Bontozoglou 1998; Nagasaki, Akiyama & Nakagawa 2002; Serifi, Malamataris & Bontozoglou 2004; Sisoev, Matar & Lawrence 2005).

The initial linear stage of the instability was considered by Benjamin (1957) and Yih (1963) who showed that the flow becomes unstable to long-waves above a critical Reynolds number which depends on the angle of inclination (for vertical inclinations, the critical Reynolds number is zero); the waves travel with a speed of twice the unperturbed flow speed at the interface. Periodic two-dimensional nonlinear waves emerge whose structure depends on the forcing frequency that produces them (see

Alekseenko, Nakoryakov & Pokusaev 1985; Liu, Paul & Gollub 1993), and in general these are susceptible to three-dimensional instabilities and ensuing spatiotemporal complexity (Joo & Davis 1992; Liu & Gollub 1993; Chang *et al.* 1994; Johnson *et al.* 1999). It is observed that the long-time behaviour of the flow is dominated by solitary wave pulses and the interactions between them, and hence a fundamental understanding of their existence and dynamics, in different physical situations is of importance. Experiments confirming the central role of solitary wave structures have been carried out by Liu & Gollub (1994), Vlachogiannis & Bontozoglou (2001) and Argyriadi, Serifi & Bontozoglou (2004).

Direct numerical simulations of the falling-film problem on flat substrates have been carried out by several investigators including Salamon, Armstrong & Brown (1994), Malamataris, Vlachogiannis & Bontozoglou (2002), Gao, Morley & Dhir (2003), Argyriadi *et al.* (2004), Gu *et al.* (2004), Kunugi & Kino (2005); calculations and experiments over wavy walls can be found in Malamataris & Bontozoglou (1999) and Vlachogiannis & Bontozoglou (2002), respectively. The computations of Malamataris *et al.* (2002) evaluate the spatial linear stability stage of the dynamics and consider in detail the velocity profiles beneath solitary waves with the finding that a strong non-parabolicity emerges in front of the main humps along with a small region of backflow. The dynamics is quite delicate and it is useful, therefore, to obtain reduced systems that can be studied in detail both numerically and analytically.

At Reynolds numbers not too far from critical, then, it is feasible to develop a long-wave nonlinear theory as in Benney (1966), Gjevik (1970) and Alekseenko *et al.* (1985), for example, giving rise to the so-called 'Benney' evolution equation. Even though this equation contains different physical mechanisms and is potentially capable of describing the nonlinear dynamics, it lacks a global existence theory for its solutions. Evidence of this can be found in numerical experiments by Pumir, Manneville & Pomeau (1983), Joo, Davis & Bankhoff (1991) and Rosenau & Oron (1992). On the other hand, it has been used successfully to describe experimental observations of three-dimensional fingering instabilities in falling films (see Diez & Kondic 2001, 2002; Kondic & Diez 2001). Reviews of falling film flows, and in particular their nonlinear analysis via long-wave models at small and moderately large Reynolds numbers, can be found in Chang (1994) and Chang & Demekhin (2002).

Weakly nonlinear analysis of the Benney equation leads to the Kuramoto–Sivashinsky (KS) equation, which deserves a special mention. This equation arises in a variety of physical problems and is one of the simplest one-dimensional evolution equations which exhibit complex dynamics. Applications include falling-film flows (Benney 1966; Sivashinsky & Michelson 1980; Shlang & Sivashinsky 1982; Hooper & Grimshaw 1985), core–annular flows (Papageorgiou, Maldarelli & Rumschitzki 1990; Coward, Papageorgiou & Smyrlis 1995) flame-front instabilities and reaction diffusion combustion dynamics (Sivashinsky 1977, 1983), chemical physics for propagation of concentration waves (Kuramoto & Tsuzuki 1975, 1976; Kuramoto 1978), and plasma physics (Cohen *et al.* 1976). The rescaled KS equation on 2π-periodic intervals contains a single parameter $\nu = (\pi/L)^2$ (here L is half of the interval on which the equation is considered) which is inversely proportional to the length of the system. The equation was extensively studied computationally (Sivashinsky & Michelson 1980; Frisch, She & Thual 1986; Hyman & Nikolaenko 1986; Hyman, Nikolaenko & Zaleski 1986; Greene & Kim 1988; Kevrekidis, Nicolaenko & Scovel 1990; Papageorgiou & Smyrlis 1991; Smyrlis & Papageorgiou 1991, 1996) as well as analytically (Il'yashenko 1992; Collet *et al.* 1993*a*, *b*; Goodman 1994; Jolly, Rosa & Temam 2000). It is established that the KS equation produces complicated dynamics in both space and time, and

when the parameter ν is small enough the solutions become chaotic. A computational verification of a period-doubling route to chaos according to the Feigenbaum scenario along with calculation of the two universal constants, can be found in Papageorgiou & Smyrlis (1991) and Smyrlis & Papageorgiou (1991, 1996).

The present work is concerned with wave formation and evolution of falling films which are additionally driven by an electric field acting normal to the plate. Perhaps the earliest known electrohydrodynamic experiment was performed by William Gilbert in the seventeenth century, who observed the formation of a conical structure on a sessile drop when a charged rod was brought above it – Taylor (1969). Most of the earlier modelling has used perfectly conducting liquids or perfect dielectrics and a review is given in Melcher & Taylor (1969). More recent work has introduced the so-called 'leaky dielectric' model to deal with poorly conducting liquids and electrolytes (see Allan & Mason 1962; Saville 1977; Russel, Saville & Schowalter 1989; Saville 1997). The possibility of controlling the film flow using a vertical electric field has been suggested by Kim, Bankoff & Miksis (1992, 1994), Bankoff, Miksis & Gwinner (1994), Bankoff, Griffing & Schluter (2002) and Griffing *et al.* (2004) in their consideration of the electrostatic liquid-film radiator. The idea is to use the reduction of pressure induced by the electric Maxwell stresses at the liquid/air interface, to reduce or stop leakage of fluid out of punctures in the outer casing of cooling equipment which is exposed to cosmic particle impacts in space applications. The theoretical study of Kim *et al.* (1992) is two-dimensional (so the holes are slits) and considers a perfect dielectric liquid and a finite-length electrode placed relatively close to the grounded infinite-plane substrate. An evolution equation is derived which is similar to the Benney equation, but contains an additional local term due to the electric field (surface tension is not included); an analogous analysis is performed for higher Reynolds numbers using the von Kármán–Pohlhausen parabolic profile approximation to obtain closure (see Chang & Demekhin 2002). Numerical solutions show reasonable agreement with direct Navier–Stokes simulations and indicate the feasibility of attaining sufficiently negative pressures in the vicinity of the electrode that can arrest leakage. The linear stability is also considered for perfectly conducting fluids and it is found that the presence of a vertical electric field reduces the critical Reynolds number below which the flow is stable. A comparison between experiment and lubrication theory (for a finite-length electrode) is made in Griffing *et al.* (2004) and agreement is reasonable. A striking experimental demonstration of the instability due to a vertical field in the absence of a shear flow can be found in Dong, de Almeida & Tsouris (2001), where the field induces the formation and protrusion of liquid columns of one liquid into a second immiscible liquid with different electrical properties. Even though the observed phenomenon is three-dimensional, a fundamental understanding of two-dimensional nonlinear interfacial electrohydrodynamics is a suitable starting point and is one of the aims of the present work. The presence of shear (see the experiments of Bankoff *et al.* 2002; Griffing *et al.* 2004) is found to nonlinearly saturate the interfacial amplitudes and this is also established by our theoretical study of the modified KS equation. An interesting analogue of shear stabilization is that of the nonlinear saturation of capillary instability in core–annular flows (see for example Papageorgiou *et al.* 1990).

Gonzalez & Castellanos (1996) considered a perfectly conducting liquid film with the upper electrode placed far from the grounded substrate. A Benney-type equation is written down which contains a non-local contribution due to the electric field above the liquid layer and the fact that the second electrode is at infinity. The form of such non-local terms has been derived formally in related horizontal electric field

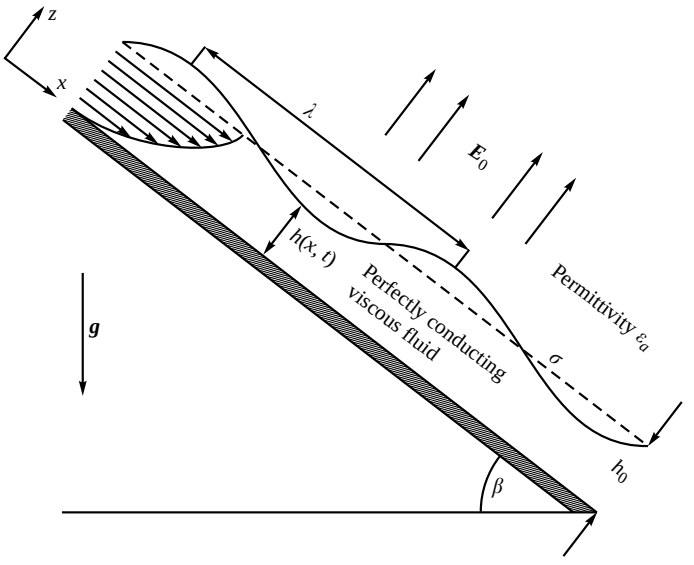

FIGURE 1. Schematic of the problem.

problems by Tilley, Petropoulos & Papageorgiou (2001), Papageorgiou & Vanden-Broeck (2004*a*, *b*). The weakly nonlinear version of this equation is a KS equation with an additional linear term due to the electric field, which enhances the instability. At sufficiently small Reynolds numbers, Gonzalez & Castellanos (1996) identify a critical electric field strength above which a mode with non-zero wavenumber first becomes unstable. They in turn use a Ginzburg–Landau weakly nonlinear expansion to establish a supercritical bifurcation. The behaviour of the flow at arbitrary electric field values was not studied and is undertaken in a systematic way in the present work. It is important also to emphasize that if the Reynolds number is sufficiently large (so that the non-electrified problem is linearly unstable to long-waves), the weakly nonlinear theory of Gonzalez & Castellanos (1996) is not possible and the problem must be addressed numerically. Therefore, there is little overlap between the present work and that of Gonzalez & Castellanos (1996). We address the modified KS equation numerically (at Reynolds numbers above and below critical). The dynamics is quite different depending on the Reynolds number, but in all cases the system evolves to mostly chaotic dynamics as the length of the system is increased.

The structure of the paper is as follows. Section 2 formulates the mathematical problem and the nonlinear interfacial boundary conditions; in § 3, we develop a formal asymptotic solution valid for long waves, and point out some associated difficulties for fully nonlinear waves, and derive the weakly nonlinear modified KS equation. In § 4, we present detailed numerical solutions and construct a fairly complete picture of the competing nonlinear dynamics (for Reynolds numbers above and below critical); some analytical results are also provided. In § 5, we present our conclusions.

2. Two-dimensional fluid flow down an inclined plane under normal electric field

2.1. *Physical model*

The physical model of a two-dimensional flow is depicted in figure 1. A Newtonian liquid of constant density ρ and viscosity μ, flows under gravity along an infinitely

long flat plate which is inclined at an angle β to the horizontal. A coordinate system (x, z) is adopted with x measuring distance down and along the plate and z distance perpendicular to it (see figure 1). The film thickness is $z = h(x, t)$ and its unperturbed value is h_0. The surface tension coefficient between the liquid and the surrounding medium is σ and the acceleration due to gravity in denoted by $\boldsymbol{g}$. The plate is taken to be an infinite electrode which, without loss of generality, is held at zero voltage potential, i.e. the electrode is grounded. Far from the plate, the electric field $\boldsymbol{E}_0$ is uniform and normal to the plate. The surrounding medium is assumed to be a perfect dielectric with permittivity ε_a, and the corresponding voltage potential in it is denoted by V. In this study, the liquid is assumed to be perfectly conducting, implying that the potential on the deformed liquid interface is zero (the electric field in the liquid is also zero). Along with the usual viscous stresses at the free surface, the electric field causes additional Maxwell stresses which can affect flow stability and the ensuing dynamics. Physically, this occurs by a reduction in pressure just beneath the interface due to the field and we wish to study systematically this effect on the nonlinear dynamics of the falling film.

2.2. *Governing equations*

Let the velocity field in the (x, z) coordinate system be $\boldsymbol{u} = (u, v)$. In what follows, we denote the liquid layer by Region I and the surrounding medium by Region II. The governing equations in Region I are the incompressible Navier–Stokes equations:

$$u_t + uu_x + vu_z = -\frac{p_x}{\rho} + \nu(u_{xx} + u_{zz}) + g\sin\beta, \tag{2.1}$$

$$v_t + uv_x + vv_z = -\frac{p_z}{\rho} + \nu(v_{xx} + v_{zz}) - g\cos\beta, \tag{2.2}$$

$$u_x + v_z = 0. \tag{2.3}$$

The potential in Region II is determined by electrostatics and the electric field can be written in terms of the gradient of the potential V as $\boldsymbol{E} = -\nabla V$. It follows that V satisfies the Laplace equation:

$$V_{xx} + V_{zz} = 0. \tag{2.4}$$

The boundary conditions are those of no slip at the wall, $u|_{z=0} = 0$, $v|_{z=0} = 0$, and a uniform field condition at infinity, $V_x \to 0$, $V_z \to -E_0$ as $z \to \infty$. At the interface $z = h(x, t)$ we must satisfy a kinematic condition, the zero (or constant) potential condition and balance of normal and tangential stresses. The out pointing unit normal and unit tangent vectors at any point on $z = h(x, t)$ are given by $\boldsymbol{n} = (-h_x, 1)/(1 + h_x^2)^{1/2}$ and $\boldsymbol{t} = (1, h_x)/(1 + h_x^2)^{1/2}$. The kinematic condition is

$$v = h_t + uh_x, \tag{2.5}$$

and noting that $\nabla V \cdot \boldsymbol{t} = 0$ is equivalent to a constant potential on the interface, yields

$$V = 0 \quad \Rightarrow \quad V_x + h_x V_z = 0 \quad \text{on} \quad z = h(x, t). \tag{2.6}$$

The components of the stress tensors in Region I are

$$T_{ij}^{\mathrm{I}} = -p\delta_{ij} + \mu\left(\frac{\partial u_i}{\partial x_j} + \frac{\partial u_j}{\partial x_i}\right), \tag{2.7}$$

and in Region II

$$T_{ij}^{\mathrm{II}} = -p_{atm}\delta_{ij} + \varepsilon_a\left(E_i E_j - \tfrac{1}{2}|\boldsymbol{E}|^2\delta_{ij}\right), \tag{2.8}$$

where p_{atm} is the constant atmospheric pressure. In this paper, we assume that $i, j = 1, 2$, $x_1 = x$, $x_2 = z$, $u_1 = u$, $u_2 = v$, and (E_1, E_2) are the components of the electric field. Note that the stresses in Region I do not have an electric part owing to the absence of a field, while those in Region II do not have a viscous part since the outer phase is assumed to be hydrodynamically passive. In general, both viscous and electrical stresses are present (for perfect dielectrics see Savettaseranee *et al.* 2003, for example). The tangential and normal stress balances at the interface take the form

$$[\boldsymbol{t}\cdot\boldsymbol{T}\cdot\boldsymbol{n}]_{\mathrm{II}}^{\mathrm{I}} = 0, \tag{2.9}$$

$$[\boldsymbol{n}\cdot\boldsymbol{T}\cdot\boldsymbol{n}]_{\mathrm{II}}^{\mathrm{I}} = \sigma\kappa, \tag{2.10}$$

where $\kappa = h_{xx}/(1+h_x^2)^{3/2}$ is the curvature of the interface. The Maxwell stresses do not contribute to the tangential stress balance unless there is a finite conductivity in either of the two phases, as in the leaky dielectric model (see for example Papageorgiou & Petropoulos 2004). This can be verified directly for the present problem by using condition (2.6) in (2.9); if, in addition, we use $u_x = -v_z$ from the continuity equation, the boundary condition (2.9) becomes

$$\left(1 - h_x^2\right)(u_z + v_x) + 4h_x v_z = 0 \quad \text{on} \quad z = h(x, t). \tag{2.11}$$

Using a similar procedure and the identity $u_z + v_x = -4h_x v_z/(1 - h_x^2)$, which follows, from (2.11), yields the following normal stress boundary condition

$$p_{atm} - p - \tfrac{1}{2}\varepsilon_a\left(1 + h_x^2\right)V_z^2 + 2\mu\frac{1 + h_x^2}{1 - h_x^2}v_z = \frac{\sigma h_{xx}}{\left(1 + h_x^2\right)^{3/2}} \quad \text{on} \quad z = h(x, t). \tag{2.12}$$

This completes the statement of the problem which, when supplemented with initial conditions, constitutes a formidable nonlinear free-boundary problem. We will proceed asymptotically and seek nonlinear evolution equations valid for long-waves. Before doing this it is useful to identify an exact (albeit unstable) solution and an appropriate non-dimensionalization.

An exact solution exists which has $h(x, t) = h_0$ with h_0 being a positive constant. This is analogous to the Nusselt solution for the non-electric case (see Nusselt 1916; Benjamin 1957) and is given by

$$\bar{u} = \frac{g\sin\beta}{2\nu}(2h_0 z - z^2), \tag{2.13}$$

$$\bar{v} = 0, \tag{2.14}$$

$$\bar{p} = p_{atm} - \tfrac{1}{2}\varepsilon_a E_0^2 - \rho g(z - h_0)\cos\beta, \tag{2.15}$$

$$\overline{V} = E_0(h_0 - z). \tag{2.16}$$

We see that the steady velocity profile is parabolic in z, while the electric potential varies linearly with z.

2.3. *Dimensionless equations*

To non-dimensionalize the equations, distances are scaled by the unperturbed depth h_0, velocities by the base velocity at the interface $u_0|_{z=h_0} \equiv U_0 = gh_0^2\sin\beta/2\nu$, the time scale is chosen to be $h_0/U_0 = 2\nu/gh_0\sin\beta$, pressure is scaled by ρU_0^2, and the unit for

the voltage potential is taken from the change in the basic potential, which is $E_0 h_0$. Introducing the following non-dimensional variables,

$$\left.\begin{aligned} x^* = \frac{1}{h_0}x, \quad z^* = \frac{1}{h_0}z, \quad t^* = \frac{U_0}{h_0}t, \\ u^* = \frac{1}{U_0}u, \quad v^* = \frac{1}{U_0}v, \quad p^* = \frac{1}{\rho U_0^2}p, \quad V^* = \frac{1}{E_0 h_0}V, \quad h^* = \frac{1}{h_0}h, \end{aligned}\right\} \tag{2.17}$$

substituting into equations (2.1)–(2.4) and the boundary conditions (2.5), (2.6), (2.11) and (2.12) and dropping the stars, provides the following non-dimensional equations and boundary conditions: In Region I, the Navier–Stokes equations become

$$u_t + uu_x + vu_z = -p_x + \frac{1}{R}(u_{xx} + u_{zz}) + \frac{2}{R}, \tag{2.18}$$

$$v_t + uv_x + vv_z = -p_z + \frac{1}{R}(v_{xx} + v_{zz}) - \frac{2}{R}\cot\beta, \tag{2.19}$$

$$u_x + v_z = 0, \tag{2.20}$$

and in Region II, we have the Laplace equation for the electric potential:

$$V_{xx} + V_{zz} = 0. \tag{2.21}$$

No slip holds at the wall, $u|_{z=0} = 0$, $v|_{z=0} = 0$ and at infinity we have

$$V_x \to 0, \; V_z \to -1 \quad \text{as} \quad z \to \infty. \tag{2.22}$$

At the interface $z = h(x, t)$, we have:

$$V = 0, \tag{2.23}$$

$$v = h_t + uh_x, \tag{2.24}$$

$$\left(1 - h_x^2\right)(u_z + v_x) + 4h_x v_z = 0, \tag{2.25}$$

$$-\tfrac{1}{2}W_e\left(1 + h_x^2\right)V_z^2 + \frac{1 + h_x^2}{1 - h_x^2}v_z + \tfrac{1}{2}R(\bar{p}_{atm} - p) = \frac{h_{xx}}{2C\left(1 + h_x^2\right)^{3/2}}, \tag{2.26}$$

where $\bar{p}_{atm} = p_{atm}/(\rho U_0^2)$ is the non-dimensional constant pressure in Region II. The other dimensionless parameters are a Reynolds number R, a capillary number C (measuring the ratio of viscous to capillary forces) and an electric Weber number W_e (measuring the ratio of electrical to gravitational forces), and are given by

$$R = \frac{U_0 h_0}{\nu} = \frac{g h_0^3 \sin\beta}{2\nu^2}, \quad C = \frac{U_0 \mu}{\sigma} = \frac{\rho g h_0^2 \sin\beta}{2\sigma}, \quad W_e = \frac{\varepsilon_a E_0^2}{\rho g h_0 \sin\beta}. \tag{2.27}$$

The exact solutions (2.13)–(2.16) are non-dimensionalized analogously, and in what follows, we write all dependent variables as the undisturbed dimensionless solution plus an arbitrary disturbance, e.g. we write $u = \bar{u}(z) + \tilde{u}$ etc. where $\bar{u}(z) = z(2 - z)$, and drop tildes in the field equations and boundary conditions (note that we use bars to denote corresponding dimensionless base solutions). For brevity, we give only the transformed boundary conditions at the interface $z = h(x, t)$:

$$V = h - 1, \tag{2.28}$$

$$v = h_t + (h(2 - h) + u)h_x, \tag{2.29}$$

$$\left(1 - h_x^2\right)(2(1 - h) + u_z + v_x) + 4h_x v_z = 0, \tag{2.30}$$

$$-\tfrac{1}{2}W_e\left[(1 - V_z)^2\left(1 + h_x^2\right) - 1\right] + \frac{1 + h_x^2}{1 - h_x^2}v_z - \cot\beta(1 - h) - \tfrac{1}{2}Rp = \frac{h_{xx}}{2C\left(1 + h_x^2\right)^{3/2}}. \tag{2.31}$$

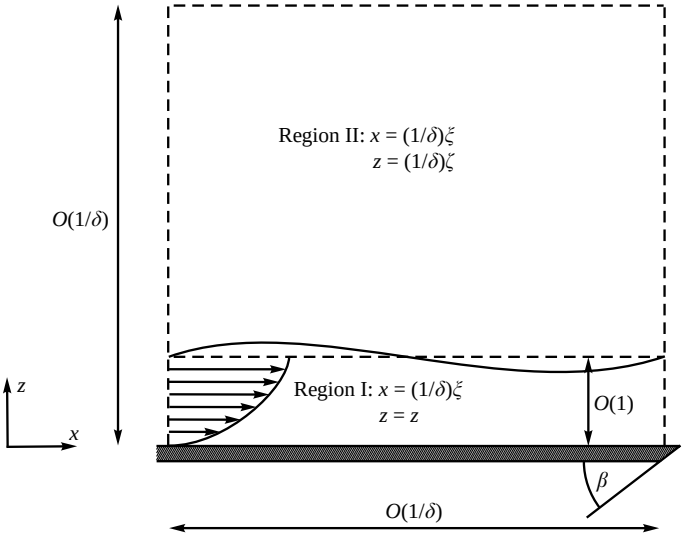

FIGURE 2. Rescaling of x and z in Regions I and II.

3. Derivation of the long-wave evolution equations

Assume that typical interfacial deformation wavelengths λ are long compared to the undisturbed thickness h_0, i.e. $\delta = h_0/\lambda \ll 1$. This condition can also be formulated as $\left|\partial h/\partial x\right| \ll 1$. Since lengths have been scaled with h_0, there is a separation of length scales in the liquid layer (Region I) and we introduce the following appropriate change of variables:

$$x = \frac{1}{\delta}\xi, \quad z = z, \quad t = \frac{1}{\delta}\tau, \quad v = \delta w. \tag{3.1}$$

The boundary conditions at the interface ($z = h(\xi, t)$) become:

$$w = h_\tau + (\bar{u} + u)h_\xi, \tag{3.2}$$

$$\left(1 - \delta^2 h_\xi^2\right)\left(\frac{\mathrm{d}\bar{u}}{\mathrm{d}z} + u_z + \delta^2 w_\xi\right) + 4\delta^2 h_\xi w_z = 0, \tag{3.3}$$

$$-\tfrac{1}{2}W_e\left[(1 - V_z)^2\left(1 + \delta^2 h_\xi^2\right) - 1\right] + \delta\frac{1 + \delta^2 h_\xi^2}{1 - \delta^2 h_\xi^2}w_z - \cot\beta(1 - h) - \tfrac{1}{2}Rp$$
$$= \frac{\delta^2 h_{\xi\xi}}{2C\left(1 + \delta^2 h_\xi^2\right)^{3/2}}. \tag{3.4}$$

Boundary condition (3.4) contains a non-local contribution since V satisfies the Laplace equation in the potential region above the fluid layer (see figure 2). Before proceeding with an asymptotic solution in Region I, we calculate the non-local contribution in (3.4) in terms of $h(\xi, t)$. To achieve this, we introduce the following independent variables in Region II:

$$x = \frac{1}{\delta}\xi, \quad z = \frac{1}{\delta}\zeta, \quad t = \frac{1}{\delta}\tau. \tag{3.5}$$

The perturbation voltage potential satisfies

$$V_{\xi\xi} + V_{\zeta\zeta} = 0, \tag{3.6}$$

$$V_\xi \to 0,\ V_\zeta \to 0 \quad \text{as} \quad \zeta \to \infty. \tag{3.7}$$

The boundary condition at the interface is

$$V|_{\zeta=\delta h} = h(\xi,\ \tau) - 1 \Rightarrow V|_{\zeta\approx 0} = h(\xi,\ \tau) - 1, \tag{3.8}$$

keeping the leading term in δ.

The solution of (3.6)–(3.8) is given by

$$V_\zeta(\xi,\ 0) = -\mathscr{H}[h_\xi], \tag{3.9}$$

and is determined by applying Cauchy's theorem to the analytic function $f(\xi + \mathrm{i}\zeta) = V_\xi - \mathrm{i}V_\zeta$, in a rectangular domain whose limiting form is the region $\zeta \geqslant 0, -\infty < \xi < \infty$ (for details see Papageorgiou & Vanden-Broeck (2004*b*); Gonzalez & Castellanos (1996) arrive at the same solution invoking the Poisson formulae). Here $\mathscr{H}$ is the Hilbert transform operator defined by:

$$\mathscr{H}[g](\xi) = \frac{1}{\pi} PV \int_{-\infty}^{\infty} \frac{g(\xi')}{\xi - \xi'}\, \mathrm{d}\xi', \tag{3.10}$$

and it is assumed that for non-periodic domains we have sufficient decay of g at infinity. PV denotes the principal value of the integral.

With the non-local contribution of the electric field known, and noting that V_z transforms to δV_ζ in terms of outer variables, boundary condition (3.4) becomes

$$-\delta W_e \mathscr{H}[h_\xi] + \delta w_z - \cot\beta(1-h) - \tfrac{1}{2}Rp + O(\delta^2) = \frac{\delta^2 h_{\xi\xi}}{2C\left(1+\delta^2 h_\xi^2\right)^{3/2}} \quad (\text{on } z=h). \tag{3.11}$$

In order to retain the effect of surface tension and the electric field in the leading-order dynamics, we chose

$$C = \delta^2 \overline{C}, \quad W_e = \frac{\overline{W}_e}{\delta}, \tag{3.12}$$

where $\overline{C}$ and $\overline{W}_e$ are order-one constants, leading to

$$p|_{z=h} = \frac{2}{R}\left[-\overline{W}_e \mathscr{H}[h_\xi] - \cot\beta(1-h) - \frac{1}{2\overline{C}} h_{\xi\xi}\right]. \tag{3.13}$$

In Region I, the appropriate asymptotic expansions are

$$u = u_0 + \delta u_1 + \delta^2 u_2 + \cdots, \qquad w = w_0 + \delta w_1 + \delta^2 w_2 + \cdots, \tag{3.14}$$

$$p = p_0 + \delta p_1 + \delta^2 p_2 + \cdots, \qquad h = H_0 + \delta H_1 + \delta^2 H_2 + \cdots. \tag{3.15}$$

In what follows, the Reynolds number R is assumed to be of order one (for long-wave analyses at large R, see Chang & Demekhin (2002) and numerous historical references therein). At the leading order we find:

$$u_0 = 2(H_0 - 1)z, \tag{3.16}$$

$$w_0 = -z^2 H_{0\xi}, \tag{3.17}$$

$$p_0 = \frac{2}{R}\left[-\overline{W}_e \mathscr{H}[H_{0\xi}] + (H_0 - 1)\cot\beta - \frac{1}{2\overline{C}} H_{0\xi\xi}\right], \tag{3.18}$$

$$H_{0\tau} + 2H_0^2 H_{0\xi} = 0. \tag{3.19}$$

The last equation represents mass conservation and is also found in the non-electrical case (Benney 1966; Lin 1974; Nakaya 1975). In general, the solution of this equation has infinite slope singularities after a finite time and the long-wave asymptotic expansion breaks down near the singularity; the usual way to proceed is to regularize the dynamics by incorporating high-order effects. We also note that for the case of weakly nonlinear evolution considered later, $H_0 \equiv 1$ satisfies (3.19) exactly, and there is no need of composite solutions that contain both order-one and order-δ terms. Proceeding to the next order, we find the following equation for H_1:

$$H_{1\tau} + H_0^2 H_{1\xi} + 2H_0 H_{0\xi} H_1 + u_1|_{z=H_0} H_{0\xi} - w_1|_{z=H_0} = 0, \tag{3.20}$$

where

$$u_1|_{z=H_0} = -\tfrac{1}{2} R H_0^2 p_{0\xi} + \tfrac{5}{6} R H_0^5 H_{0\xi} + 2H_0 H_1, \tag{3.21}$$

$$w_1|_{z=H_0} = \tfrac{1}{3} R H_0^3 p_{0\xi\xi} + \tfrac{1}{2} R H_0^2 H_{0\xi} p_{0\xi} - \tfrac{71}{30} R H_0^5 H_{0\xi}^2 - \tfrac{8}{15} R H_0^6 H_{0\xi\xi} - H_0^2 H_{1\xi}, \tag{3.22}$$

$$p_0 = \frac{2}{R}\left[-\overline{W}_e \mathscr{H}[H_{0\xi}] + (H_0 - 1)\cot\beta - \frac{1}{2\overline{C}} H_{0\xi\xi}\right]. \tag{3.23}$$

Using these expressions in (3.20) casts the latter into the more compact form:

$$H_{1\tau} + \left[2H_0^2 H_1 - \tfrac{1}{3} R H_0^3 p_{0\xi} + \tfrac{8}{15} R H_0^6 H_{0\xi}\right]_\xi = 0. \tag{3.24}$$

A regularized equation for the new dependent variable $H = H_0 + \delta H_1$ can now be sought by adding δ times equation (3.20) to equation (3.19). The resulting regularized equation is given by

$$H_\tau + \left[\tfrac{2}{3} H^3 + \delta\left(\tfrac{8}{15} R H^6 - \tfrac{2}{3}\cot\beta H^3\right) H_\xi + \frac{\delta}{3\overline{C}} H^3 H_{\xi\xi\xi} + \frac{2\delta}{3}\overline{W}_e H^3 \mathscr{H}[H_{\xi\xi}]\right]_\xi = 0, \tag{3.25}$$

and it has been verified (the calculations are not included here) that it is correct to $O(\delta^2)$. This equation was derived by Gonzalez & Castellanos (1996) using an intuitive approach rather than formal asymptotics. It is an electrostatically modified version of the nonlinear interfacial models of Lin (1974) and Nakaya (1975) and the extensive analytical and numerical study of Pumir *et al.* (1983). The latter study is particularly interesting because it shows that equation (3.25) with $\overline{W}_e = 0$ supports solitary as well as heteroclinic travelling waves. In addition, numerical solutions of the initial-value problem provide strong evidence that solutions for all time may not exist for all values of the parameters. One such calculation corresponds to our parameters $R = 13, \cot\beta = 5, \overline{C} = 1/2000$, and is found to blow up in a finite time, τ_s say; a self-similar structure is postulated in the form

$$H \sim (\tau_s - \tau)^{-1/9} G\left(\xi/(\tau_s - \tau)^{1/6}\right),$$

where G is a scaling function that was not calculated. In addition to the evidence that global existence of solutions is unlikely, we see from equations (3.19) and (3.24) that, in general, $H_{0\xi}$ and higher derivatives become infinite in finite time and this also holds for H_1 and its derivatives. In fact if $H_\xi = H_{0\xi} + \delta H_{1\xi}$, for example, is to remain bounded (as is the case for most parameter values) then H_1 and higher terms become unbounded in finite time. We have verified that the neglected order-δ^2 terms that lead to (3.25) contain H_1 and these will become as large as the retained terms even when H remains smooth. We must proceed iteratively, then, writing $H = \sum_{j=0}^{n} \delta^j H_j$, $n = 2, 3, \ldots$, and showing that an evolution equation is obtained which is correct to $O(\delta^{n+1})$, for each n. This calculation has not been carried out for $n \geqslant 3$. In the light of these difficulties, then, we construct rational asymptotic solutions that do not

have a δ-dependence. This is achieved by looking for weakly nonlinear corrections to $H_0 = 1$ which solves (3.19) exactly – see also Sivashinsky & Shlang (1982) for the related problem of film flow down a vertical column when the column radius is asymptotically large compared to the film thickness. It is also important to note that when the plate is horizontal, $\beta = 0$, a fully nonlinear long-wave evolution equation which is independent of δ, appears at leading order (see Oron, Davis & Bankhoff 1997).

3.1. *Weakly nonlinear evolution*

We seek a consistent asymptotic evolution of long-waves by imposing $H_0(\xi, \tau) \equiv 1$. We write $H = 1 + \alpha(\delta)\eta$ where $\alpha(\delta) = o(\delta^{1/2})$ and $\eta = O(1)$. Substituting into (3.25) we obtain, correct to order δ,

$$\eta_\tau + 2\eta_\xi + 4\alpha\eta\eta_\xi - \frac{2D}{3}\delta\eta_{\xi\xi} + \frac{\delta}{3\overline{C}}\eta_{\xi\xi\xi\xi} + \frac{2\overline{W}_e}{3}\delta\mathscr{H}[\eta_{\xi\xi\xi}] = 0, \tag{3.26}$$

where $D = \cot\beta - 4R/5$. The advective term $2\eta_\xi$ is removed by a Galilean transformation and a canonical equation arises from (3.26) when the following change of variables is used:

$$\xi - 2\tau = \frac{1}{(2\overline{C}|D|)^{1/2}}x, \quad \delta\tau = \frac{3}{4\overline{C}D^2}t, \quad \eta = \frac{\delta}{6\alpha}(2\overline{C}|D|^3)^{1/2}u, \tag{3.27}$$

to obtain

$$u_t + uu_x \pm u_{xx} + u_{xxxx} + \gamma\mathscr{H}[u_{xxx}] = 0. \tag{3.28}$$

Note that u from now on represents the scaled interfacial amplitude and is unrelated to previous dependent variables; $\gamma = 2\overline{W}_e\overline{C}/|D|^{1/2}$ is a positive constant and the plus sign in front of u_{xx} is taken if D is negative while the minus sign is taken if D is positive. As a weakly nonlinear approximation of (3.25), equation (3.28) is valid for $u = o(\delta^{-1/2})$. When the electric field is absent, i.e. $W_e = 0$, and $D < 0$, the canonical equation is the Kuramoto–Sivashinsky (KS) equation (see Pumir *et al.* 1983 and § 1):

$$u_t + uu_x + u_{xx} + u_{xxxx} = 0. \tag{3.29}$$

3.2. *Linear stability*

Linearizing (3.28) about $u = 0$ gives $u_t \pm u_{xx} + u_{xxxx} + \gamma\mathscr{H}[u_{xxx}] = 0$ which has normal mode solutions proportional to $\exp(ikx + st)$ if the dispersion relation

$$s(k) = -k^4 + \gamma|k|^3 \pm k^2, \tag{3.30}$$

is satisfied (here we use the following result, $\widehat{\mathscr{H}[u]}(k) = -i\,\mathrm{sign}\,k\,\hat{u}(k)$ where hats denote a Fourier transform). This dispersion relation was also given by Gonzalez & Castellanos (1996) in an unscaled form. The case with the positive sign corresponds to $D < 0$ ($R > R_c = 5\cot\beta/4$) and gives a band of unstable modes for $0 < k < (\gamma + \sqrt{\gamma^2 + 4})/2$. As γ increases, the size of the band and the corresponding maximum growth rate, increase. Representative results are shown in figure 3.

If $D > 0$ ($R < R_c$), we obtain the negative sign in (3.30), and as pointed out in Gonzalez & Castellanos (1996), there are two sub-cases: (i) $\gamma \leqslant 2$ where all modes are stable, i.e. $s(k) \leqslant 0$ for all k, and, (ii) $\gamma > 2$ where there appears a band of unstable waves extending from $k = (\gamma - \sqrt{\gamma^2 - 4})/2$ to $k = (\gamma + \sqrt{\gamma^2 - 4})/2$. Typical results are shown in figure 3.

In both cases, the electric field is destabilizing. The weakly nonlinear stability in the vicinity of $\gamma = 2$ was carried out by Gonzalez & Castellanos (1996) where a

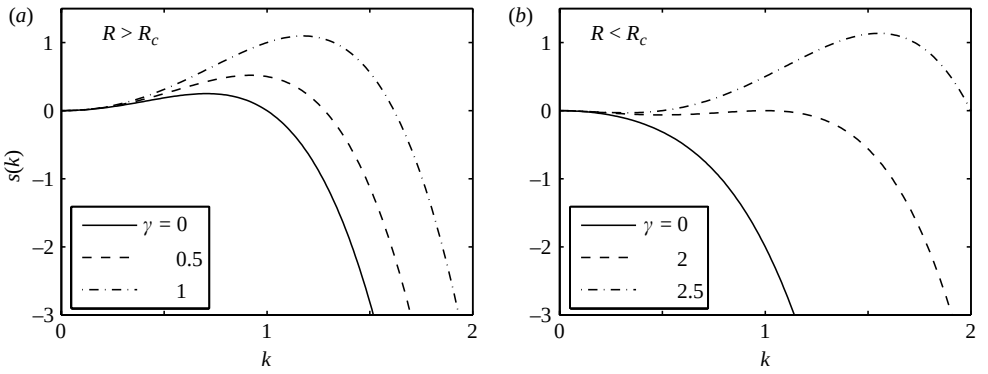

FIGURE 3. Changes in the dispersion relation due to the electric field. (*a*) corresponds to the flow above the critical Reynolds number, (*b*) below the critical Reynolds number.

Ginzburg–Landau equation admitting supercritical states was derived. The present work has very little overlap with that study since we are interested in the dynamics well beyond critical in Case II; we also study Case I which is not amenable to a similar weakly nonlinear theory.

4. Spatio-temporal dynamics: regular and chaotic solutions

Linear theory predicts that sufficiently long-waves are unstable and that the electric field increases the instability band to include relatively shorter waves. For the KS equation, it is established (numerically and analytically) that nonlinearity acts to saturate the instability (negative diffusion and fourth-derivative damping) to produce a host of rich dynamical behaviour: steady states, Hopf bifurcations to time-periodic solutions, period doubling cascades to chaos according to the Feigenbaum scenario, chaotic attractors with coexisting stable multi-modal fixed points, etc. The electric field enhances the instability and the objective of this section is a systematic mapping of its effect on the dynamics as compared to those known for the KS equation. Note also that Case II above, is not the KS equation when $\gamma = 0$, and in what follows we present evidence that chaotic states emerge in this case also if γ is sufficiently large. This suggests that the electric field can be used to produce interfacial turbulence at small or zero Reynolds numbers where all disturbances would otherwise be damped. We are not aware of any controlled experiments that have shown such behaviour, and the present calculations could be useful in suggesting such studies.

Consider (3.28) on a finite interval $[-L, L]$ with periodic boundary conditions; L measures the size of the system and controls the number of unstable modes present (in the context of the KS equation). We can normalize equation (3.28) to 2π-periodic domains using the rescaling

$$\bar{t} = (\pi/L)^2 t, \quad \bar{x} = (\pi/L)x, \quad \bar{u} = (L/\pi)u, \tag{4.1}$$

which (on dropping the bars) casts the equation into

$$u_t + uu_x \pm u_{xx} + \nu u_{xxxx} + \mu \mathscr{H}[u]_{xxx} = 0, \tag{4.2}$$

where $\nu = (\pi/L)^2$ and $\mu = (\pi/L)\gamma$. Periodic initial conditions are also prescribed (see later).

We used two different numerical methods. The first method implements a linear propagator so that the linear part of the operator is done exactly in Fourier space

and the stiffness is removed (see for example Trefethen 2000). For example, if hats denote Fourier transforms, and $\hat{U} = \mathrm{e}^{-s(k)t}\hat{u}$, the equation becomes

$$\hat{U}_t + \tfrac{1}{2}\mathrm{i}\mathrm{e}^{-s(k)t}k\widehat{u^2} = 0, \tag{4.3}$$

where $s(k)$ is the spectrum from linear theory (see above). Using a pseudospectral representation of derivatives, equation (4.3) becomes an ordinary differential equation (ODE) for $\hat{U}$ (for each k), and is solved with a fourth-order Runge–Kutta method.

The second method is a Fourier–Galerkin one. Let $\hat{u}_k(t)$ be the Fourier coefficients of $u(x, t)$, i.e.

$$u(x, t) = \sum_{k=-\infty}^{\infty} \hat{u}_k(t)\mathrm{e}^{\mathrm{i}kx}. \tag{4.4}$$

Equation (4.2) is equivalent to the following infinite dimensional system of ODEs

$$\frac{\mathrm{d}\hat{u}_k(t)}{\mathrm{d}t} = (-\nu k^4 + \mu|k|^3 \pm k^2)\hat{u}_k(t) - \tfrac{1}{2}\mathrm{i}k \sum_{k_1+k_2=k} \hat{u}_{k_1}(t)\hat{u}_{k_2}(t). \tag{4.5}$$

These equations were integrated using the Matlab integrator ode23tb for stiff differential equations with variable step size to ensure stability and accuracy. The modes $\hat{u}_k$ are only computed for $|k| < K_{max}$, all other $\hat{u}_k$ being set to 0, with K_{max} chosen so that the neglected modes have magnitudes less than 10^{-15}. The value of K_{max} depends on μ and ν and, in most of the computations described here, it has a value of 30 or less.

The initial condition used is

$$u_0(x) = \frac{1}{10}\sum_{k=1}^{10}(\alpha_k \cos(kx) + \beta_k \sin(kx)), \tag{4.6}$$

where the coefficients α_k, β_k, $k = 1, 2, \ldots, 10$, are chosen randomly in the interval [0, 1]. The methods were implemented and tested for a very large number of the values of the parameters ν and μ. For the first method, for example, the space discretization ranged from 128 to 512 modes and the time step was taken to be 10^{-3} or smaller with typical maximum integration times of 100–1000 time units. A variety of diagnostics is used to determine the form of the solution – these include the tracking of the maxima and minima of the L^2 norm of the solution, return maps using these, and Fourier transforms of large time series data. Such diagnostics have been used successfully in the past for different problems (see Smyrlis & Papageorgiou 1991, 1996; Hall & Papageorgiou 1999; Blyth, Hall & Papageorgiou 2003). Typically, for each set of parameters, we track the time evolution of the profile, its energy (L^2-norm) and its Fourier modes. The evolution of the energy was used to classify various attractors. For example, for steady or steady-state travelling waves, the energy reaches a constant value at large times, and for periodic attractors, the energy is a periodic function of time. For chaotic solutions, the energy becomes highly oscillatory and information is extracted by numerically constructing return maps and studying their geometry – e.g. self-similar folding behaviour is strong evidence of a chaotic attractor – see references above.

4.1. *Numerical results, Case I: modified Kuramoto–Sivashinsky equation*

All our numerical results indicate that the solutions remain bounded as t becomes large. A proof of such a result is available for the KS equation (see § 1) and this

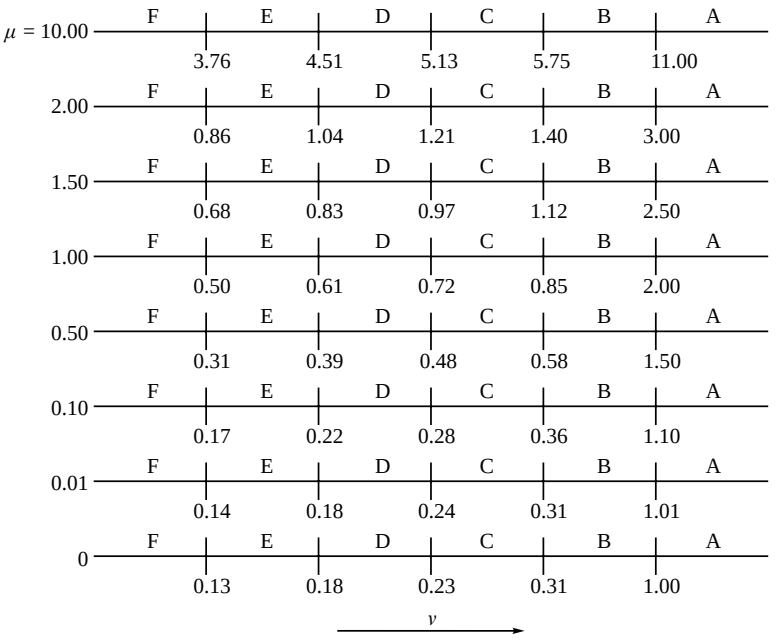

FIGURE 4. Schematic of the various attractors. A, solution decays to zero; B, unimodal steady state; C, unimodal steady-state travelling wave; D, periodic hormoclinic bursts; E, bimodal steady state; F, complicated dynamics including windows of time periodic attractors with period doubling, multimodal steady-state attractors, homoclinic bursts, and chaotic oscillations.

has been extended to the modified KS equation (Duan & Ervin 1998; Tseluiko & Papageorgiou 2006). In what follows we provide a quantitative description of the different attractors as ν and μ vary (decreasing ν corresponds to an increased length of the system and increasing μ corresponds to an increased applied voltage difference).

It was also observed numerically that as the coefficient μ of the integral term goes to zero, the solutions of the modified KS equation converge in L^2 to the corresponding solutions of the usual KS equation. At $\mu = 0$, we recover the results obtained for the usual KS equation; this also confirms the accuracy of the numerical simulations.

In figure 4, we depict a summary of the results for different values of μ as ν decreases. The two-parameter phase space is quite large and we confine our results to an overall description of the dynamical features rather than a detailed study of individual attractors. The letters A–F are used to identify windows of the parameter ν for various attractors for fixed but moderate values of μ. As μ increases, the qualitative dynamics remains the same, but the windows A–F widen in ν. The boundaries in the (ν, μ)-plane that separate the attractors A–F are shown in figure 5, from which it is seen that all follow linear laws with slopes larger than or equal to one. The right-most boundary separating attractors A and B has been established analytically, but we do not have an explanation for the linear behaviour of the other boundaries at present. We note that the lines 'fan' out and do not cross. A brief description of the different attractors along with sample numerical results is given next.

In the attractor labelled A, the solutions decay to zero as time increases and a trivial steady state is achieved (note that the initial condition has zero spatial mean). This result can be proved analytically for any μ, using the Poincaré

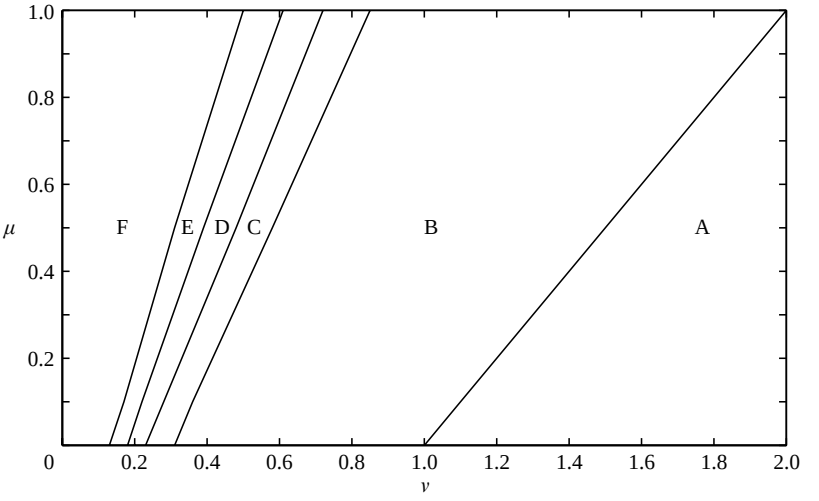

FIGURE 5. The boundaries between attractors in the (ν, μ)-plane. Case I.

inequality (see Temam 1988):

$$\int_{-\pi}^{\pi} g^2 \, \mathrm{d}x \leqslant \int_{-\pi}^{\pi} g_x^2 \, \mathrm{d}x, \tag{4.7}$$

for periodic functions of period 2π. In fact, we can prove the following. If $\nu > 1 + \mu$ then the solutions of (4.2) converge to zero (in L^2_{per}) as t goes to infinity. (Here L^2_{per} is the subspace of $L^2(-\pi, \pi)$ consisting of periodic functions with period 2π.) To prove this, we multiply equation (4.2) by u, integrate from $-\pi$ to π with respect to x and use periodicity to obtain

$$\frac{1}{2}\frac{\mathrm{d}}{\mathrm{d}t}\int_{-\pi}^{\pi} u^2 \, \mathrm{d}x = \int_{-\pi}^{\pi} u_x^2 \, \mathrm{d}x - \nu \int_{-\pi}^{\pi} u_{xx}^2 \, \mathrm{d}x + \mu \int_{-\pi}^{\pi} u_x \mathscr{H}[u]_{xx} \, \mathrm{d}x. \tag{4.8}$$

Using the Cauchy–Schwartz inequality and the the fact that the Hilbert transform commutes with derivatives, and its L^2 norm is equal to the L^2 norm of the function on which it operates, we can estimate

$$\begin{aligned}\int_{-\pi}^{\pi} u_x \mathscr{H}[u]_{xx} \, \mathrm{d}x &\leqslant \frac{1}{2}\int_{-\pi}^{\pi} u_x^2 \, \mathrm{d}x + \frac{1}{2}\int_{-\pi}^{\pi} \mathscr{H}[u]_{xx}^2 \, \mathrm{d}x \\ &= \frac{1}{2}\int_{-\pi}^{\pi} u_x^2 \, \mathrm{d}x + \frac{1}{2}\int_{-\pi}^{\pi} \mathscr{H}[u_{xx}]^2 \, \mathrm{d}x, \\ &= \frac{1}{2}\int_{-\pi}^{\pi} u_x^2 \, \mathrm{d}x + \frac{1}{2}\int_{-\pi}^{\pi} u_{xx}^2 \, \mathrm{d}x. \end{aligned} \tag{4.9}$$

Using this in (4.8) along with inequality (4.7) for $g = u_x$, gives

$$\frac{1}{2}\frac{\mathrm{d}}{\mathrm{d}t}\int_{-\pi}^{\pi} u^2 \, \mathrm{d}x \leqslant (1 + \mu - \nu)\int_{-\pi}^{\pi} u_{xx}^2 \, \mathrm{d}x. \tag{4.10}$$

The Poincaré inequality (4.7) also implies

$$\int_{-\pi}^{\pi} u_{xx}^2 \, \mathrm{d}x \geqslant \int_{-\pi}^{\pi} u^2 \, \mathrm{d}x. \tag{4.11}$$

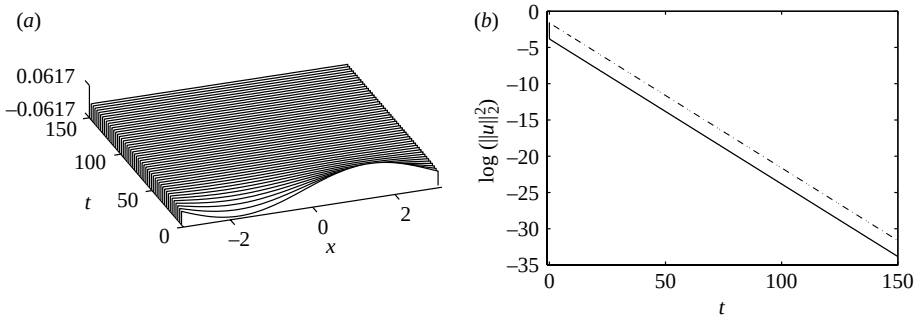

FIGURE 6. Window A, $\mu = 0.5$, $\nu = 1.6$. (*a*) The evolution of the profile; (*b*) the semi-log plot of the evolution of the energy, verifying the decay predicted by the theoretical estimate (4.13). —, graph of $\log(||u||_2^2)$; –·–, line with the slope $= 2(1 + \mu - \nu)$.

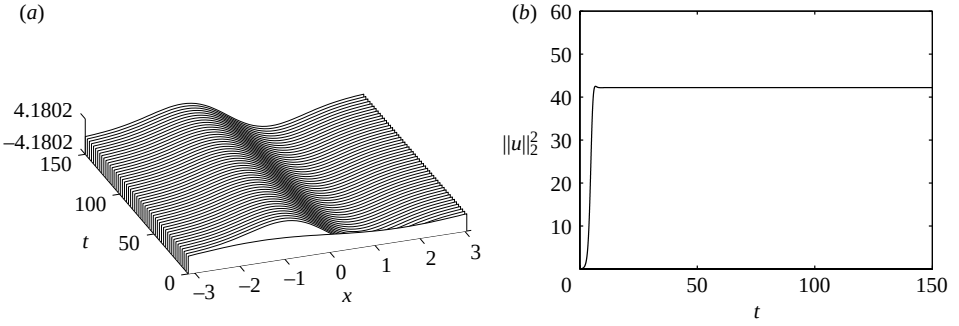

FIGURE 7. Window B. Unimodal steady state for $\mu = 0.5$, $\nu = 0.7$. (*a*) The evolution of the profile; (*b*) the evolution of the energy.

Hence, for $\nu > 1 + \mu$ we have

$$\frac{1}{2}\frac{\mathrm{d}}{\mathrm{d}t}\int_{-\pi}^{\pi} u^2\,\mathrm{d}x \leqslant (1 + \mu - \nu)\int_{-\pi}^{\pi} u^2\,\mathrm{d}x. \tag{4.12}$$

Therefore there exists a non-negative constant C such that

$$\int_{-\pi}^{\pi} u^2\,\mathrm{d}x \leqslant C\mathrm{e}^{2(1+\mu-\nu)t}. \tag{4.13}$$

This implies that $\|u\|_2 \to 0$ as $t \to \infty$, as required. This fact is fully reflected in the results of figure 4 and hence serves as an additional check on the numerical work. A sample run which quantifies the rate of decay, is given in figure 6 for $\mu = 0.5$, $\nu = 1.6$; it is verified numerically, therefore, that the decay is exponential with a rate given by the estimate (4.13).

For $\nu < 1 + \mu$, the trivial solution bifurcates to provide a branch of unimodal (2π-periodic) steady states – window B in figure 4. These are globally attracting and are stable (the latter observation is based on our time-dependent numerical procedure). Figure 7 depicts the evolution of the profile and the corresponding energy for $\nu = 0.7$, $\mu = 0.5$. The solution reaches its steady state in about 10 time units and the long integration to 150 time units provides strong evidence of stability. The size of the windows of attractor B increase as μ increases, but at the same time, the lower boundary of attractor B shifts to larger values of ν. For example, when $\mu = 0$, the

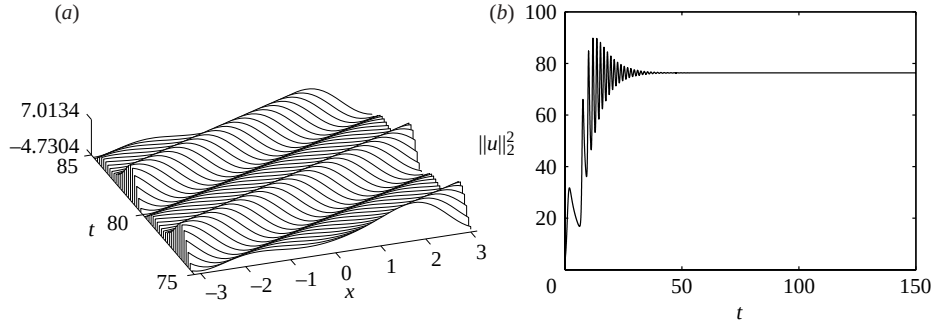

FIGURE 8. Window C. Unimodal steady-state travelling wave for $\mu = 0.5$, $\nu = 0.5$. (*a*) The evolution of the profile; (*b*) the evolution of the energy.

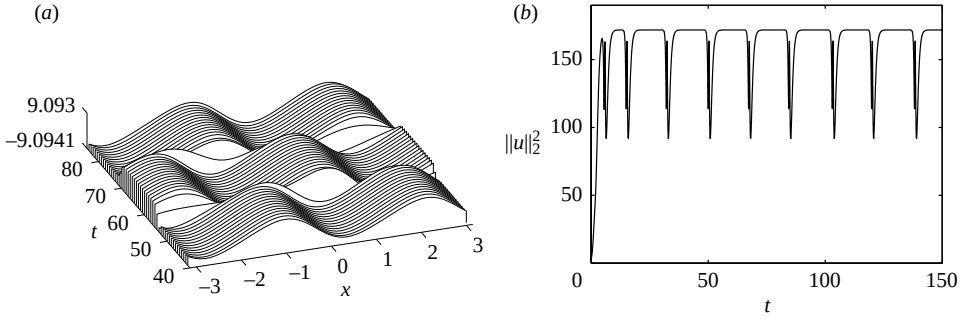

FIGURE 9. Window D. Periodic homoclinic bursts for $\mu = 0.5$, $\nu = 0.45$. (*a*) The evolution of the profile; (*b*) the evolution of the energy.

lower boundary of B is at $\nu \approx 0.31$ while for $\mu = 0.5$ the corresponding value is $\nu \approx 0.5$. This behaviour persists for higher values of μ and for different attractors as is seen in figure 4. Physically, the implication is that as the voltage potential difference is increased, more complicated dynamics emerge as compared to the KS equation.

As ν decreases further, solutions in attractor B lose stability through a Hopf bifurcation to travelling-wave states. These nonlinear travelling waves are unimodal (i.e. they have spatial periods of 2π). For fixed μ, the speed of the travelling waves increases monotonically as ν is decreased. Typical results from this window are shown in figure 8 for $\mu = 0.5$, $\nu = 0.5$. It is observed from the evolution of the energy that the initial transient stages of the solution are oscillatory in time, indicating the presence of a time-periodic attractor in the vicinity of these values of the parameters. These transient oscillations become longer lived as ν is decreased (for all μ discussed here), and indeed another Hopf bifurcation takes place, this time producing temporally homoclinic bursts. It is found that the solution between bursts is a bimodal fixed point (i.e. the shortest spatial period is π – alternatively, all the energy is carried by the even Fourier modes). The bursts are identical (this has been checked by studying the phase plane of the energy, for example), but the time between bursts is not constant and so the solution is not strictly time periodic – this is also true for the KS equation (Smyrlis & Papageorgiou 1996). The minimum time between bursts (after transients disappear) increases as ν is decreased for a fixed value of μ. Typical results are shown in figure 9 which depicts the profile evolution and the corresponding energy evolution for $\mu = 0.5$, $\nu = 0.45$.

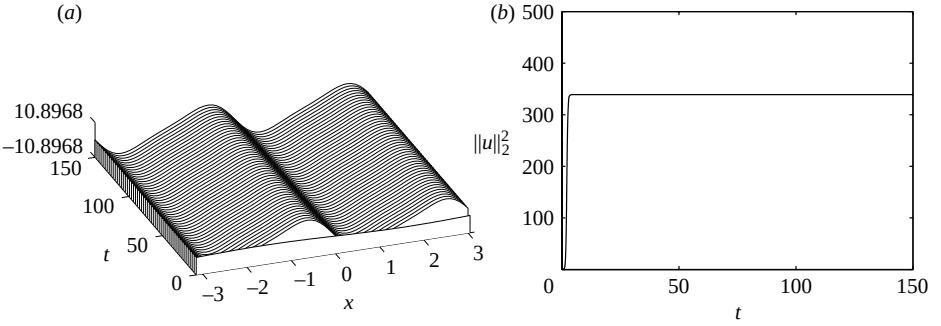

FIGURE 10. Window E. Bimodal steady state for $\mu = 0.5$, $\nu = 0.35$. (a) The evolution of the profile; (b) the evolution of the energy.

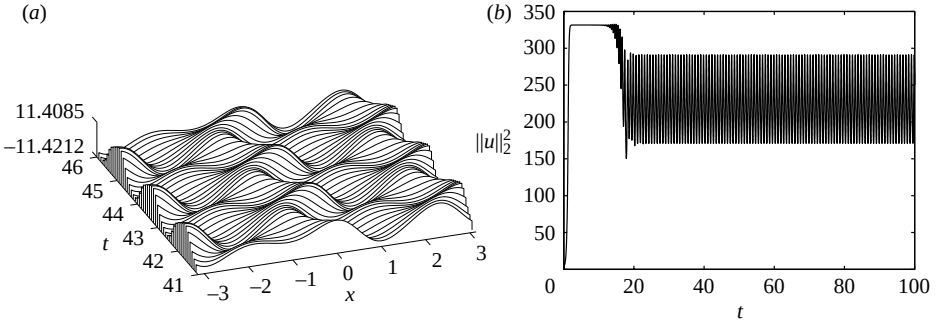

FIGURE 11. Window F. Time periodic attractor for $\mu = 0.5$, $\nu = 0.298$. (a) The evolution of the profile; (b) the evolution of the energy.

Further decrease of ν leads to a new bimodal fixed-point attractor denoted by E in figure 4. This attractor emerges from attractor D as the period of oscillation of the homoclinic bursts becomes increasingly larger. We have checked the stability of these fixed-point solutions by integrating to very large times. Typical results are depicted in figure 10 for $\mu = 0.5$, $\nu = 0.35$.

In the initial stages of window F, the bimodal steady states lose stability and a Hopf bifurcation to time periodic solutions takes place. As ν decreases, the period increases monotonically until a period doubling takes place. Sample results are given in figure 11 which depicts the profile evolution and the corresponding energy evolution for $\mu = 0.5$ and $\nu = 0.298$. The period has undergone several period doublings and its current value is approximately 0.8. This pattern of subharmonic bifurcations follows the Feigenbaum scenario in much the same way as for the non-electric case (see, for example, Papageorgiou & Smyrlis 1991; Smyrlis & Papageorgiou 1991, 1996). We have not carried out an exhaustive study to estimate the Feigenbaum universal constants as was done in the papers above, but have confirmed the trend and the geometric contraction of time-periodic windows of increasingly larger periods. Just beyond the accumulation point (in ν for fixed μ), the solutions become attracted to chaotic homoclinic bursts which are spaced apart at roughly equal time intervals, the profile between bursts being bimodal. Representative solutions are given in figure 12 for $\mu = 0.5$ and $\nu = 0.29$. In this case the time between chaotic bursts is approximately 44 time units. As ν decreases further, the dynamics becomes more complicated and we have computed solutions in small windows supporting multimodal fixed points,

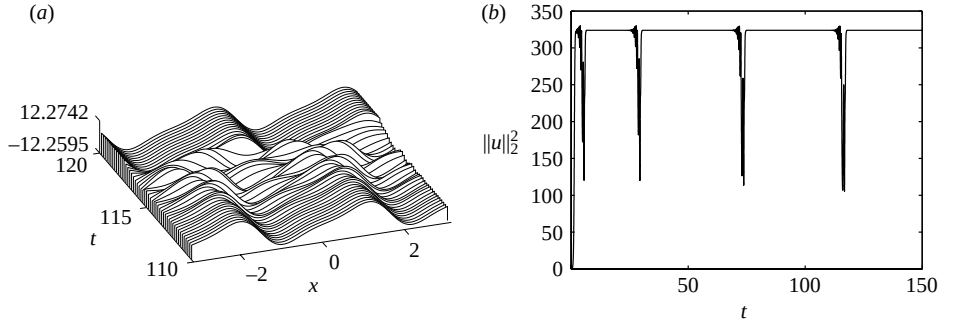

FIGURE 12. Window F. Chaotic homoclinic bursts for $\mu = 0.5$, $\nu = 0.29$. (*a*) The evolution of the profile; (*b*) the evolution of the energy.

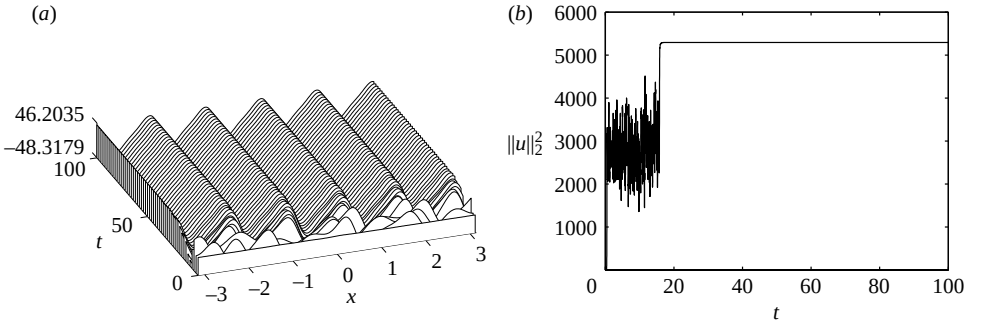

FIGURE 13. Window F. Multimodal steady attractor for $\mu = 0.5$, $\nu = 0.1$. (*a*) The evolution of the profile; (*b*) the evolution of the energy.

for example. The strongest attractors appear to be chaotic, however, in line with the dynamics of the KS equation. Such features are illustrated in figure 13 which contains computations for $\mu = 0.5$ and $\nu = 0.1$ (the value of ν is substantially below the accumulation point that heralds the beginning of the first chaotic attractor). The solution is a pentamodal fixed-point (the spatial period is $2\pi/5$ and only the Fourier modes which are multiples of 5 appear in the spectrum) and the trough to crest distance is relatively large, approximately equal to 95 units. Such waves have been observed in KS calculations also (see Frisch *et al.* 1986; Smyrlis & Papageorgiou 1996). We note also that the transient to the steady state is about 20 time units and appears to be chaotic, but fixed-point solutions are more attracting in this particular region of the phase space (this statement is based on the fact that our initial conditions are chosen randomly). Finally, in figure 14 we reduce the value of ν to 0.05 and the emerging solution is chaotic for the duration of the run which is 100 time units.

4.2. *Numerical results, Case II: damped modified Kuramoto–Sivashinsky equation*

In this case, the minus sign is picked in the canonical equation (4.2) and if $\mu \leqslant 2\sqrt{\nu}$, the growth rate is non-positive and all waves are stable. A necessary condition for instability is $\mu^2 > 4\nu$ in which case all waves in the interval $(k_-,\ k_+)$ are unstable where

$$k_\pm = \frac{\mu \pm \sqrt{\mu^2 - 4\nu}}{2\nu}. \tag{4.14}$$

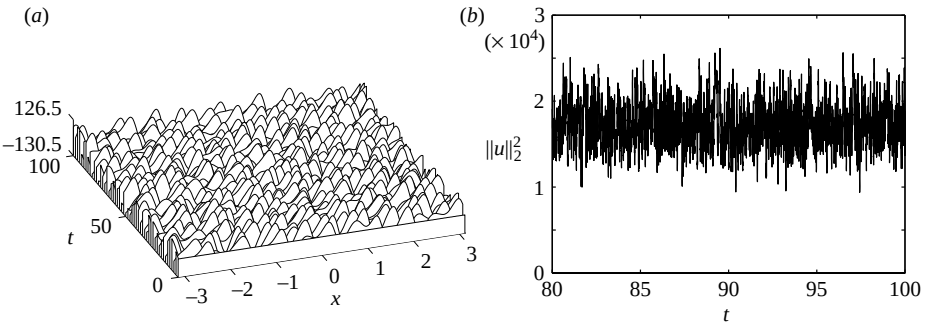

FIGURE 14. Window F. Chaotic oscillations for $\mu = 0.5$, $\nu = 0.05$. (*a*) The evolution of the profile; (*b*) the evolution of the energy.

Clearly, if μ is fixed and ν is sufficiently large, all modes are stable. In fact, modifying the analysis of § 4.1, we can prove that $\|u\|_2 \to 0$ as $t \to \infty$ as long as

$$\nu > \mu - 1. \tag{4.15}$$

The main difference is the minus sign in the first term on the right-hand side of (4.8) and the expression of the bound in terms of $\|u_x\|_2$ first rather than $\|u_{xx}\|_2$. It has been established numerically that the bound (4.15) is sharp as long as $\mu > 2$, that is, trivial solutions are guaranteed at large times in this case. When $\mu < 2$, the analysis is modified by introducing the Poincaré inequality for multimodal solutions. This is guided by numerical solutions as well as linear theory for the finite periodic domains of interest here, as we describe next.

Consider the countably infinite set of points (μ, ν) where the modes $k = 1, 2, \ldots$ first become unstable (note that we are restricted to integer k owing to the particular choice of periodic boundary conditions). These must lie on the curve $\mu = 2\sqrt{\nu}$ (see above), and must satisfy

$$k_- = k_+ = m, \quad m = 1, 2, \ldots. \tag{4.16}$$

Solving, we obtain

$$\nu = \frac{1}{m^2}, \quad \mu = \frac{2}{m}, \quad m = 1, 2, \ldots, \tag{4.17}$$

which shows that if we fix $\mu = 2/m$ and increase ν above $1/m^2$, a trivial solution emerges at large times. To obtain a sharp stability boundary we must consider values of ν and μ away from these neutral points. For example, if $k = m$ is to be unstable, then we require it to be contained in the interval (k_-, k_+), that is

$$k_- < m, k_+ > m \quad \Rightarrow \quad \mu > m\nu + \frac{1}{m}. \tag{4.18}$$

The boundary of these regions is seen to be the tangent curve to $\mu = 2\sqrt{\nu}$ at each of the neutral monochromatic modes (4.17) for each $m = 1, 2, \ldots$. The stability boundary is therefore a polygonal curve made up of the segments $\mu = m\nu + 1/m$ so that the curve with the smallest μ is kept. The points of intersection of two such curves at successive values m and $m + 1$, say, indicate points (ν, μ) where the modes $k = m$ and $k = m + 1$ are neutral simultaneously. These intersections are given by

$$\mu = \frac{2m+1}{m(m+1)}, \quad \nu = \frac{1}{m(m+1)}, \quad m = 1, 2, \ldots. \tag{4.19}$$

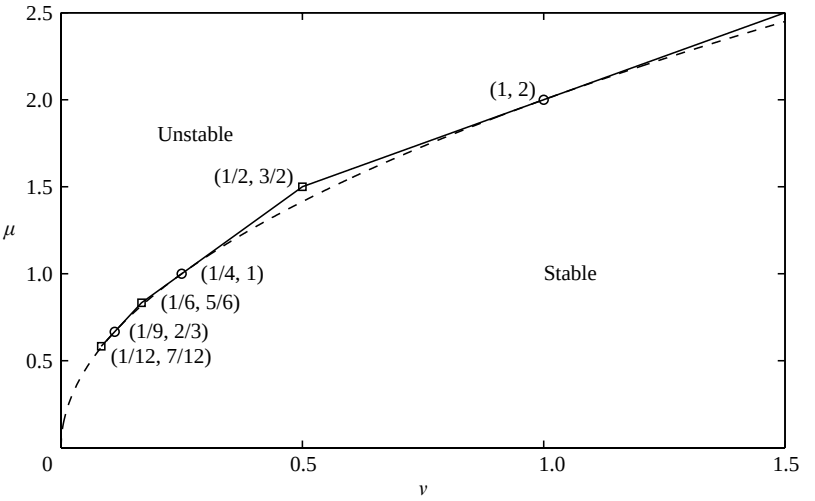

FIGURE 15. The first bifurcation boundary in the (ν, μ)-plane. The first three segments of the boundary are shown. Circles (from top to bottom) denote points where the modes $k = 1, 2, 3$ are neutral, respectively. Squares (from top to bottom) are points where the modes $k = 1, 2$, $k = 2, 3$ and $k = 4, 5$ are neutral.

Note also that the $m = 1$ line becomes the sharp first bifurcation boundary $\mu = \nu + 1$ that holds for $\mu > 2$ analysed earlier. In figure 15, we show the first three segments of this boundary – higher elements become increasingly difficult to distinguish from the parabolic curve owing to the geometric clustering of the higher neutral points as m increases.

Bifurcations in the neighbourhood of the circles produce m-modal non-uniform steady states of period $2\pi/m$ as m increases (that is as $\mu, \nu \to 0$). For large ν trivial solutions emerge when (4.15) is satisfied. In general, the bifurcated solutions near this curve are unimodal steady states since the $k = 1$ mode becomes active first. The bifurcation near the points (4.19) marked by squares in figure 15 produces unimodal behaviour owing to the nonlinear interaction of modes which differ by unit wavenumber. These stability results provide some explanations for the results of numerical experiments described next.

We have carried out extensive numerical experiments and the results are collected in figure 16. As described above, the limit $\mu, \nu \to 0$ deserves separate attention since we expect a host of interesting dynamical behaviour such as multimodal attractors and resonant wave interactions. We do not pursue this limit further in the present work, but note the run having $\mu = 1$ in figure 16. This run is chosen to correspond with the dynamics originating from the bifurcation point denoted by an open circle at (1/4, 1) in figure 15. The run fixes $\mu = 1$ and decreases ν below 0.25. As discussed above, a bimodal steady state is expected since a wave with $k = 2$ is marginally stable at (1/4, 1). The numerical results show that a supercritical bifurcation takes place and a bimodal steady state is supported in the region $0.227 \leqslant \nu < 0.25$, indicated by the letter E. Just below $\nu = 0.227$, the dynamics become complicated with chaotic solutions emerging as labelled by the attractor F. Two other values, $\mu = 0.8$ and 1.4 fall within this 'small' μ, ν region. For $\mu = 0.8$, a non-trivial steady state bifurcates at $\nu = (0.8 - 1/3)/3 \approx 0.1556$ (this comes from the segment defined by (4.18) for $m = 3$ – see also figure 15). The neutral wavenumber has $k = 3$, but the long-time dynamics computed here indicate attractor F behaviour. One explanation for this

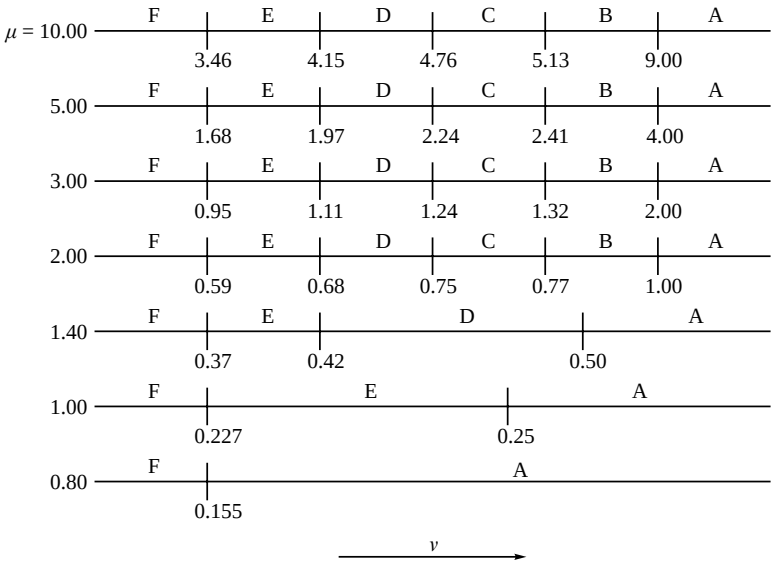

FIGURE 16. Schematic of the attractors for Case II. A, solution decay to zero; B, unimodal steady state; C, unimodal steady-state travelling wave; D, periodic hormoclinic bursts; E, bimodal steady state; F, complicated dynamics including windows of time periodic attractors with period doubling, multimodal steady-state attractors, homoclinic bursts, and chaotic oscillations.

is that due to the geometric contraction of the segments comprising the polygonal stability boundary, it is increasingly difficult to find attractors which are supported on windows of diminishing size. A bifurcation analysis of this limit is the subject of future work. Similar reasoning can be applied to the other numerical example that has $\mu = 1.4$. The bifurcation is now through a $k = 2$ neutral mode and the sequence of computed windows begins with periodic homoclinic bursts, to bimodal steady states to dynamics in attractor F.

The other results in figure 15 are at values of $\mu \geqslant 2$, and they all have similar bifurcation paths, namely the sequence of attractors A $\rightarrow$ B $\rightarrow$ C $\rightarrow$ D $\rightarrow$ E $\rightarrow$ F, in much the same way as was discovered for Case I earlier. These cases lie outside the small μ, ν bifurcation scenario given above and all bifurcations are unimodal with $k = 1$ being the neutral mode. In addition, subwindow lengths increase as μ increases, the behaviour being linear and similar to that depicted in figure 5. Ultimately, however, our numerical results indicate that for any μ, the dynamics are attracted to chaotic states if ν is sufficiently small. This happens at small electric fields also and generic dynamical phenomena are observed.

5. Conclusions

We have derived and used long-wave model equations to study the behaviour of falling films when a normal electric field is present. Through a combination of analysis and computations, we have established the spatio-temporal interfacial dynamics when the amplitudes are small, but a nonlinearity is present. This has been done by considering solutions of a modified KS equation, the modification being a non-local term due to the electric field. There are two canonical evolution equations, one valid for Reynolds numbers above critical, $R > 5\cot\beta/4$, and one below critical;

both canonical equations depend on two parameters: $\nu = (\pi/L)^2 > 0$ where L is the length of the system, and $\mu = 2\nu^{1/2}\overline{W}_e\overline{C}/|\cot\beta - \frac{4}{5}R|^{1/2} \geqslant 0$, which is proportional to the reduced electric Weber number $\overline{W}_e$ (this in turn is proportional to the square of the applied electric field, see (2.27)). In the absence of an electric field, the evolution equation above critical Reynolds numbers is the KS equation which has a band of linearly unstable waves for all values of $\nu < 1$. Below critical, however, there are no linearly unstable waves and instability is possible only if μ is sufficiently large. We have established numerically, that as long as a uniform constant interface is linearly unstable, then the large-time dynamics depends on the value of ν: trivial states emerge if $\nu > \mu + 1$ or $\nu > \mu - 1$ for flows above/below critical, respectively; as ν is decreased, different attractors are found supporting non-uniform steady-state solutions, time-periodic solutions and chaotic solutions if ν is sufficiently small. Our results predict that interfacial chaos can be achieved at zero Reynolds numbers also, when fluid inertia is completely absent – the electric field provides the energy input for this phenomenon.

The work of DTP was supported by the National Science Foundation Grant number DMS-0072228. DT acknowledges support from NJIT.

REFERENCES

Alekseenko, S., Nakoryakov, V. & Pokusaev, B. 1985 Wave formation on a vertical falling liquid film. *AIChE J.* **31**, 1446–1460.

Allan, R. S. & Mason, S. G. 1962 Particle behaviour in shear and electric fields. I. deformation and burst of fluid drops. *Proc. R. Soc. Lond.* A **267**, 45–61.

Argyriadi, K., Serifi, K. & Bontozoglou, V. 2004 Nonlinear dynamics of inclined films under low-frequency forcing. *Phys. Fluids* **16**, 2457–2468.

Bankoff, S., Griffing, E. & Schluter, R. 2002 Use of an electric field in an electrostatic liquid film radiator. *Ann. NY Acad. Sci.* **974**, 1–9.

Bankoff, S., Miksis, M. & Gwinner, H. K. R. 1994 Design considerations for the rotating electrostatic liquid-film radiator. *Nucl. Engng Des.* **149**, 441–447.

Benjamin, T. B. 1957 Wave formation in laminar flow down an inclined plane. *J. Fluid Mech.* **2**, 554–574.

Benney, D. J. 1966 Long waves on liquid films. *J. Math. Phys.* **45**, 150–155.

Binny, A. M. 1957 Experiments on the onset of wave formation on a film of water flowing down a vertical plane. *J. Fluid Mech.* **2**, 551–555.

Blyth, M., Hall, P. & Papageorgiou, D. 2003 Chaotic flows in pulsating cylindrical tubes: a class of exact Navier–Stokes solutions. *J. Fluid. Mech.* **481**, 187–213.

Bontozoglou, V. 1998 A numerical study of interfacial transport to a gas-sheared wavy liquid. *Intl J. Heat Mass Transfer* **41**, 2297–2305.

Chang, H.-C. 1994 Wave evolution on a falling film. *Annu. Rev. Fluid Mech.* **26**, 103–136.

Chang, H.-C., Cheng, M., Demekhin, E. & Kopelevich, D. 1994 Secondary and tertiary excitation of three-dimensional patterns on a falling film. *J. Fluid. Mech.* **270**, 251–275.

Chang, H.-C. & Demekhin, E. 2002 *Complex Wave Dynamics on Thin Films*. Elsevier.

Cohen, B. I., Krommes, J. A., Tang, W. M. & Rosenbluth, M. N. 1976 Non-linear saturation of the dissipative trapped ion mode by mode coupling. *Nucl. Fusion* **16**, 971–992.

Collet, P., Eckmann, J.-P., Epstein, H. & Stubbe, J. 1993*a* Analyticity for the Kuramoto–Sivashinsky equation. *Physica* D **67**, 321–326.

Collet, P., Eckmann, J.-P., Epstein, H. & Stubbe, J. 1993*b* A global attracting set for the Kuramoto–Sivashinsky equation. *Commun. Math. Phys.* **152**, 203–214.

Coward, A. V., Papageorgiou, D. T. & Smyrlis, Y. S. 1995 Nonlinear stability of oscillatory core–annular flow: a generalized Kuramoto–Sivashinsky equation with time periodic coefficients. *Z. Angew. Math. Phys.* **46**, 1–39.

Diez, J. & Kondic, L. 2001 Contact line instabilities of thin liquid films. *Phys. Rev. Lett.* **86**, 632–635.

Diez, J. & Kondic, L. 2002 Computing three-dimensional thin film flows including contact lines. *J. Comput. Phys.* **183**, 274–306.

Dong, J., de Almeida, V. & Tsouris, C. 2001 Formation of liquid columns on liquid–liquid interfaces under applied electric fields. *J. Colloid Interface Sci.* **242**, 327–336.

Duan, J. & Ervin, V. J. 1998 Dynamics of a non-local Kuramoto–Sivashinsky equation. *J. Diffl Equat.* **143**, 243–266.

Dukler, A. 1976 The role of waves in two phase flow: some new understanding. *Chem. Engng Educ.* Summer, 108–138.

Frisch, U., She, Z. S. & Thual, O. 1986 Viscoelastic behaviour of cellular solutions to the Kuramoto–Sivashinsky model. *J. Fluid Mech.* **186**, 221–240.

Gao, D., Morley, N. & Dhir, V. 2003 Numerical simulation of wavy falling film flow using VOF method. *J. Comput. Phys.* **192**, 624–642.

Gjevik, B. 1970 Occurrence of finite-amplitude surface waves on falling liquid films. *Phys. Fluids* **13**, 1918–1925.

Gonzalez, A. & Castellanos, A. 1996 Nonlinear electrohydrodynamic waves on films falling down an inclined plane. *Phys. Rev.* E **53**, 3573–3578.

Goodman, J. 1994 Stability of the Kuramoto–Sivashinsky and related systems. *Commun. Pure Appl. Maths* **47**, 293–306.

Greene, J. M. & Kim, J.-S. 1988 The steady states of the Kuramoto–Sivashinsky equation. *Physica* D **33**, 99–120.

Griffing, E., Bankoff, S., Miksis, M. & Schluter, R. 2004 Electrohydrodynamics of thin flowing films. Preprint.

Gu, F., Liu, C., Yuan, X. & Yu, G. 2004 CFD simulation of liquid film flow on inclined plates. *Chem. Engng Technol.* **27**, 1099–1104.

Hall, P. & Papageorgiou, D. 1999 The onset of chaos in a class of exact Navier–Stokes solutions. *J. Fluid. Mech.* **393**, 59–87.

Hooper, A. P. & Grimshaw, R. 1985 Nonlinear instability at the interface between two fluids. *Phys. Fluids* **28**, 37–45.

Hyman, J. M. & Nikolaenko, B. 1986 The Kuramoto–Sivashinsky equations, a bridge between PDEs and dynamical systems. *Physica* D **18**, 113–126.

Hyman, J. M., Nikolaenko, B. & Zaleski, S. 1986 Order and complexity in the Kuramoto–Sivashinsky model of turbulent interfaces. *Physica* D **23**, 265–292.

Il'yashenko, J. S. 1992 Global analysis of the phase portrait for the Kuramoto–Sivashinsky equation. *J. Dyn. Diffl Equat.* **4**, 585–615.

Johnson, M., Schluter, R., Bankoff, S. & Miksis, M. 1999 Experimental study of rivulet formation on an inclined plate by fluorescent imaging. *J. Fluid Mech.* **394**, 339–354.

Jolly, M. S., Rosa, R. & Temam, R. 2000 Evaluating the dimension of an inertial manifold for the Kuramoto–Sivashinsky equation. *Adv. Diffl Equat.* **5**, 31–66.

Joo, S. & Davis, S. 1992 Instabilities of three-dimensional viscous falling films. *J. Fluid Mech.* **242**, 529–547.

Joo, S., Davis, S. H. & Bankhoff, S. 1991 Long-wave instabilities of heated falling films: two-dimensional theory of uniform layers. *J. Fluid Mech.* **230**, 117.

Kapitza, P. L. & Kapitza, S. P. 1949 Wave flow of thin fluid layers of liquids. *Sov. Phys., J. Exp. Theor. Phys.* **19**, 105–120.

Kevrekidis, I. G., Nicolaenko, B. & Scovel, C. 1990 Back in the saddle again: a computer assisted study of the Kuramoto–Sivashinsky equation. *SIAM J. Appl. Maths* **50**, 760–790.

Kim, H., Bankoff, S. & Miksis, M. 1992 The effect of an electrostatic field on film flow down an inclined plane. *Phys. Fluids* A **4**, 2117–2130.

Kim, H., Bankoff, S. & Miksis, M. 1994 The cylindrical electrostatic liquid-film radiator for heat rejection in space. *Trans. ASME J. Heat Transfer* **116**, 986–992.

Kondic, L. & Diez, J. 2001 Pattern formation in the flow of thin films down an incline: constant flux configuration. *Phys. Fluids* **13**, 3168–3184.

Kunugi, T. & Kino, C. 2005 DNS of falling film structure and heat transfer via Mars method. *Comput. Struct.* **83**, 455–462.

Kuramoto, Y. 1978 Diffusion-induced chaos in reaction systems. *Prog. Theor. Phys. Suppl.* **64**, 346–367.

Kuramoto, Y. & Tsuzuki, T. 1975 On the formation of dissipative structures in reaction diffusion systems. *Prog. Theor. Phys.* **54**, 687–699.

Kuramoto, Y. & Tsuzuki, T. 1976 Persistent propogation of concentration waves in dissipative media far from thermal equilibrium. *Prog. Theor. Phys.* **55**, 356–369.

Lin, S. P. 1974 Finite amplitude sideband stability of a viscous film. *J. Fluid Mech.* **63**, 417–429.

Liu, J. & Gollub, J. 1993 Onset of spatially chaotic waves on flowing films. *Phys. Rev. Lett.* **70**, 2289–2292.

Liu, J. & Gollub, J. 1994 Solitary wave dynamics of film flows. *Phys. Fluids* **6**, 1702–1712.

Liu, J., Paul, J. & Gollub, J. 1993 Measurements of the primary instabilities of film flows. *J. Fluid Mech.* **250**, 69–101.

Malamataris, N. & Bontozoglou, V. 1999 Computer aided analysis of viscous film flow along an inclined wavy wall. *J. Comput. Phys.* **154**, 372–392.

Malamataris, N., Vlachogiannis, M. & Bontozoglou, V. 2002 Solitary waves on inclined films: flow structure and binary interactions. *Phys. Fluids* **14**, 1082–1094.

Melcher, J. & Taylor, G. I. 1969 Electrohydrodynamics: a review of the role of interfacial shear stresses. *Annu. Rev. Fluid Mech.* **1**, 111.

Nagasaki, T., Akiyama, H. & Nakagawa, H. 2002 Numerical analysis of flow and mass transfer in a falling liquid film with interfacial waves. *Thermal Sci. Engng* **10**, 1231–1240.

Nakaya, C. 1975 long-waves on a thin fluid layer flowing down an inclined plane. *Phys. Fluids* **18**, 1407–1412.

Nusselt, W. 1916 Die Oberflachenkondesation des Wasserdampfes. *Z. Ver. Deut. Indr.* **60**, 541–546.

Oron, A., Davis, S. H. & Bankhoff, S. 1997 Long-scale evolution of thin liquid films. *Rev. Mod. Phys.* **69**, 931–980.

Papageorgiou, D. T., Maldarelli, C. & Rumschitzki, D. S. 1990 Nonlinear interfacial stability of core–annular film flow. *Phys. Fluids* A **2**, 340–352.

Papageorgiou, D. T. & Petropoulos, P. G. 2004 Generation of interfacial instabilities in charged electrified viscous liquid films. *J. Engng Maths* **50**, 223–240.

Papageorgiou, D. T. & Smyrlis, Y. S. 1991 The route to chaos for the Kuramoto–Sivashinsky equation. *Theor. Comput. Fluid Dyn.* **3**, 15–42.

Papageorgiou, D. T. & Vanden-Broeck, J.-M. 2004*a* Antisymmetric capillary waves in electrified fluid sheets. *Eur. J. Appl. Maths* **15**, 609–623.

Papageorgiou, D. T. & Vanden-Broeck, J.-M. 2004*b* Large-amplitude capillary waves in electrified fluid sheets. *J. Fluid. Mech.* **508**, 71–88.

Pumir, A., Manneville, P. & Pomeau, Y. 1983 On solitary waves running down an inclined plane. *J. Fluid Mech.* **135**, 27–50.

Rosenau, P. & Oron, A. 1992 Bounded and unbounded patterns of the Benney equation. *Phys. Fluids* A **4**, 117.

Russel, W. B., Saville, D. A. & Schowalter, W. R. 1989 *Colloidal Dispersions*. Cambridge University Press.

Salamon, T. R., Armstrong, R. C. & Brown, R. A. 1994 Traveling waves on vertical films: numerical analysis using the finite element method. *Phys. Fluids* **6**, 2202–2220.

Savettaseranee, K., Papageorgiou, D. T., Petropoulos, P. G. & Tilley, B. 2003 The effect of electric fields on the rupture of thin viscous films by van der Waals forces. *Phys. Fluids* **15**, 641–652.

Saville, D. A. 1977 Electrokinetic effects with small particles. *Annu. Rev. Fluid Mech.* **9**, 321–337.

Saville, D. A. 1997 Electrohydrodynamics: the Taylor–Melcher leaky dielectric model. *Annu. Rev. Fluid Mech.* **29**, 2764.

Serifi, K., Malamataris, N. & Bontozoglou, V. 2004 Transient flow and heat transfer phenomena in inclined wavy films. *Intl J. Therm. Sci.* **43**, 761–767.

Shlang, T. & Sivashinsky, G. I. 1982 Irregular flow of a liquid film down a vertical column. *J. Phys.* **43**, 459–466.

Sisoev, G., Matar, O. & Lawrence, C. 2005 Absorption of gas into a wavy falling film. *Chem. Engng Sci.* **60**, 827–838.

Sivashinsky, G. & Shlang, T. 1982 Irregular flow of a liquid down a vertical column. *J. Phys. Paris* **43**, 459–466.

Sivashinsky, G. I. 1977 Nonlinear analysis of hydrodynamic instability in laminar flames. Part 1. *Acta Astronaut.* **4**, 1176–1206.

Sivashinsky, G. I. 1983 Instabilities, pattern formation, and turbulence in flames. *Annu. Rev. Fluid Mech.* **15**, 179–199.

Sivashinsky, G. I. & Michelson, D. M. 1980 On irregular wavy flow on liquid film down a vertical plane. *Prog. Theor. Phys.* **63**, 2112–2114.

Smyrlis, Y. S. & Papageorgiou, D. T. 1991 Predicting chaos for the infinite dimensional dynamical systems: the Kuramoto–Sivashinsky equation, a case study. *Proc. Natl Acad. Sci. USA* **88**, 11 129–11 132.

Smyrlis, Y. S. & Papageorgiou, D. T. 1996 Computational study of chaotic and ordered solutions of the Kuramoto–Sivashinsky equation. *ICASE Rep.* 96-12, pp. 1–32.

Taylor, G. I. 1969 Electrically driven jets. *Proc. R. Soc. Lond.* A **313**, 453–475.

Temam, R. 1988 *Infinite-Dimensional Dynamical Systems in Mechanics and Physics*. Springer.

Tilley, B., Petropoulos, P. & Papageorgiou, D. 2001 Dynamics and rupture of planar electrified liquid sheets. *Phys. Fluids* **13**, 3547–3563.

Trefethen, L. N. 2000 *Spectral Methods in Matlab*. Society for Industrial and Applied Mathematics Philadelphia, PA.

Tseluiko, D. & Papageorgiou, D. T. 2006 A global attracting set for nonlocal Kuramoto-Sivashinsky equations arising in interfacial electrohydrodynamics. *Eur. J. Appl. Maths* (submitted).

Vlachogiannis, M. & Bontozoglou, V. 2001 Observations of solitary wave dynamics of film flows. *J. Fluid Mech.* **435**, 191–215.

Vlachogiannis, M. & Bontozoglou, V. 2002 Experiments on laminar film flow along a periodic wall. *J. Fluid Mech.* **457**, 133–156.

Yih, C.-H. 1963 Stability of liquid flow down an inclined plane. *Phis. Fluids* **6**, 321–334.

Yoshimura, P., Nosoko, T. & Nagata, T. 1996 Enhancement of mass transfer into a falling laminar liquid film by two-dimensional surface waves – some experimental observations and modeling. *Chem. Engng Sci.* **51**, 1231–1240.